ACS Catalysis

Research Article

pubs.acs.org/acscatalysis

Experimental and Theoretical Study of *n*-Butanal Self-Condensation over Ti Species Supported on Silica

David G. Hanna, Sankaranarayanapillai Shylesh, Yi-Pei Li, Siddarth Krishna, Martin Head-Gordon, and Alexis T. Bell*

Department of Chemical and Biomolecular Engineering, University of California, Berkeley, California 94720, United States

Supporting Information

ABSTRACT: The effects of the coordination environment and connectivity of Ti on the rate of *n*-butanal self-condensation over Ti-silica catalysts were investigated. Ti was introduced in two ways, either during the synthesis of mesoporous SBA-15 or via grafting onto amorphous silica with a disordered pore structure. The connectivity of Ti was then characterized by XANES, UV−vis, and Raman spectroscopy. For the lowest Ti loadings, the Ti is found to be predominantly in isolated monomeric species, irrespective of the manner of sample preparation, and as the Ti loading is increased, a progressively larger fraction of Ti is present in oligomeric species and anatase nanoparticles. The turnover frequency for butanal condensation decreased monotonically with increasing Ti loading, and the apparent activation energy increased from 60 kJ mol^{-1} for monomeric species to 120 kJ mol^{-1} for oligomeric species. A kinetic H/D isotope effect was observed over isolated titanol and Ti dimer catalysts suggesting that α-H abstraction is the rate-determining step. This conclusion is supported by theoretical analysis of the reaction mechanism. In agreement with experimental results, the calculated activation barrier for alkanal condensation over a Ti dimer is roughly two times greater than that over Ti-OH sites. The cause for this difference was explained by energy decomposition analysis of the enolate formation step which showed that there is a large energetic penalty for the substrate to distort over the Ti−O−Ti dimer than the Ti-OH monomer.

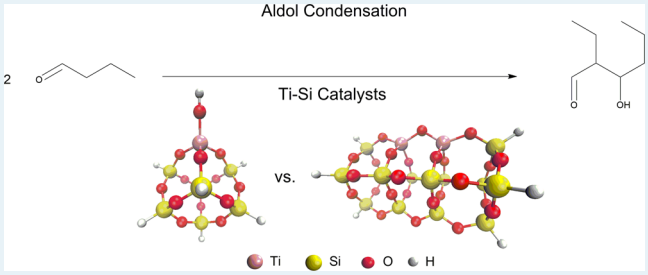

KEYWORDS: *n-butanal, aldol condensation, titanium, coordination environment, kinetics, DFT*

1.0. INTRODUCTION

Aldol condensation of aldehydes has become a subject of considerable interest because this reaction enables the formation of carbon−carbon bonds in compounds used as chemical intermediates and alternative fuels. For example, ~3 × 10^6 tons of the hydrogenated aldol product 2-ethylhexanol are produced annually for use as a plasticizer, solvent, or diesel additive,[1,2] and this product can be upgraded via esterification to produce a diesel fuel with a high cetane number.[3,4] The production of 2-ethylhexanol is generally carried out by aldol condensation of *n*-butanal and the subsequent hydrogenation of the resulting 2-ethylhexenal.

Previous studies have shown that acid−base bifunctionality plays a crucial role in the catalysis of aldol condensation.[5−9] Bulk metal oxides are promising heterogeneous aldol condensation catalysts due to the presence of robust Lewis acid and Brønsted base pairs. In particular, the anatase phase of titanium dioxide has been shown to be active and selective for aldol condensation.[10] IR studies of acetaldehyde adsorbed onto anatase reveal a significant shift in the carbonyl vibrations from 1722 to 1691 cm^{-1}, indicating that the carbonyl group is strongly bound to Lewis acidic Ti sites.[11] Strong adsorption of the aldehyde polarizes the C═O bond causing the α proton to become more acidic, thereby facilitating its subsequent H-abstraction, a key step in the mechanism of aldol condensation.[8] Barteau and co-workers have shown that the activity of the TiO_2 (001) surface for the aldol condensation of acetaldehyde increases as more surface oxygen sites are exposed via progressive oxidation of the surface.[12] This suggests that the surface oxygen acts as a Brønsted base in abstracting the α proton of the aldehyde. Anatase is thus an active catalyst for aldol condensation due to its ability to adsorb the aldehyde at Lewis acid Ti sites and abstract the α-proton at the Brønsted basic surface oxygen sites. Barteau and co-workers have also reported that the selectivity for aldol condensation of acetaldehyde is higher on the {114}-faceted (001) surface of rutile, which exposes 4, 5, and 6-coordinate Ti, than on the {011} facet, which exposes only 5-coordinate Ti (59% and 31%, respectively).[13] However, anatase was found to have even higher selectivity (75%) and activity for this reaction.[13] It is, therefore, evident that the coordination of Ti in titania has a strong effect on the activity and selectivity of Ti sites for aldol condensation.

The purpose of this study was to elucidate the role of the local coordination and connectivity of Ti sites on the activity of these sites for aldol condensation. Silica−titania catalysts with a

Received: May 22, 2014
Revised: July 15, 2014
Published: July 21, 2014

   dx.doi.org/10.1021/cs500704b | ACS Catal. 2014, 4, 2908−2916

well-defined active site were synthesized by incorporating Ti into the framework of SBA-15. These catalysts were characterized by XANES, UV−vis, and Raman spectroscopy, and then the kinetics of *n*-butanal self-condensation were investigated in order to determine the effects of coordination environment. It was observed that isolated, tetrahedrally coordinated titanol sites are more active than tetrahedrally coordinated Ti dimer species and octahedrally coordinated Ti sites present on the dispersed nanoparticles of anatase. The insights gained from the current study demonstrate the importance of Ti coordination and connectivity on the activity of Ti species as catalysts for the self-condensation of *n*-butanal.

2.0. EXPERIMENTAL AND THEORETICAL METHODS

2.1. Catalyst Synthesis. Titanium was incorporated into the framework of SBA-15 by direct hydrothermal synthesis. Tetraethoxysilane (TEOS, Aldrich) and titanium isopropoxide (Aldrich) were used as the Si and Ti sources, respectively, and Pluronic P123 triblock (Aldrich) copolymer was used as the structure-directing agent. In a typical synthesis procedure, 4.0 g of P123 was added to 70.0 mL of 0.2 M HCl solution to yield a transparent solution at 313 K. Then, 9.0 g of tetraethoxysilane and the required amount of titanium isopropoxide (Si/Ti molar ratio = 5−50) were added dropwise, and the resulting gel mixture was stirred for another 24 h. The gel was then crystallized at 393 K for 24 h. The final solid was filtered, washed with water, and dried at 383 K overnight. Finally, the samples were calcined at 823 K for 6 h. These catalysts are referred to as *x*-Ti−SBA-15, where *x* denotes the dispersion of titanium (atoms nm^{-2}).

Catalysts were also synthesized by incipient-wetness impregnation. Mesoporous SBA-15 (850 $m^2\ g^{-1}$, average pore diameter 60 Å)[14] was impregnated with either $Ti(O^iPr)_4$ (Aldrich, 99.999%) or Cp_2TiCl_2 (Aldrich, 97%) dissolved in toluene (Alfa Aesar, anhydrous 99.8% pure). In a typical synthesis procedure, a titanium loading of 0.45 wt % was achieved using roughly 30 mg $(g\ support)^{-1}$ of precursor in the solution. These catalysts are referred to as 0.07−Ti-Pr/SBA-15 and 0.07-Ti-Cp/SBA-15. Amorphous SiO_2 with a disordered pore structure (Silicycle, 500 $m^2\ g^{-1}$, average pore diameter 60 Å) was pretreated at 373 or 1023 K and was then impregnated using $Ti(O^iPr)_4$. These catalysts are referred to as 0.07-Ti-Pr/SiO_2-373K and 0.07-Ti-Pr/SiO_2-1023K. All impregnated catalysts were dried at 393 K for 12 h and calcined in 100 $cm^3\ min^{-1}$ of air (Praxair) for 823 K for 6 h.

2.2. Measurements of Catalyst Activity. Measurements of reaction rates were performed in a 6.35 mm OD quartz tube containing an expanded section (∼12.7 mm OD, ∼20 mm length). A plug of quartz wool was placed below the catalyst bed to hold the powder in place. The reactor was heated by a ceramic furnace with external temperature control, and the catalyst bed temperature was measured with a K-type thermocouple sheathed in a quartz capillary placed in direct contact with the catalyst bed.

Prior to reaction, the catalyst was heated to the reaction temperature at a rate of 2 K min^{-1} in pure He (Praxair, 99.999%) flowing at 150 $cm^3\ min^{-1}$ at STP. The feed to the reactor consisted of *n*-butanal (TCI, 98%) and He (Praxair, 99.999%). For kinetic isotope experiments, *n*-butanal-2,2-d_2 (CDN Isotopes, 98%) was used as the feed. A filled 1 mL syringe connected to a syringe pump (Cole-Palmer, 74900 series) was used to inject *n*-butanal into a heated port through which He was continuously flowing. All experiments were carried out at a total gas pressure of 1 atm. The total gas flow rate was typically 150 $cm^3\ min^{-1}$ at STP. Using these conditions, the conversion of aldehyde was always less than 10%. Reaction products were analyzed using an Agilent 6890N gas chromatograph containing a bonded and cross-linked (5%-phenyl)-methylpolysiloxane capillary column (Agilent, HP-1) connected to a flame ionization detector (FID).

2.3. Characterization. Ti content was determined by inductively coupled plasma optical emission spectroscopy (ICP-OES) conducted at Galbraith Laboratories in Knoxville, TN.

Nitrogen adsorption isotherms were performed using a Micromeritics Gemini VII surface area and pore volume analyzer. The specific surface area and pore size were calculated using the Brunauer−Emmet−Teller (BET) equation and Barrett−Joyner−Halenda (BJH) equations.

X-ray absorption spectroscopy (XAS) measurements were performed at the Advanced Photon Source at Argonne National Laboratory (ANL) on beamline 10-BM. Measurements were performed at the Ti K-edge. The Ti edge energy was taken as the first inflection point of the main absorption peak. The energy was referenced to a pure Ti foil placed between the two ionization chambers located after the sample. The catalysts and reference materials, TiO_2 anatase (Aldrich) and titanium silicate-1 (TS-1), were diluted with boron nitride, an inert and relatively X-ray transparent material, in order to achieve an absorbance of ∼2.5 because such an absorbance provides the optimal signal-to-noise ratio.[15] Samples were placed in a controlled-atmosphere cell, heated to 473 K in the presence of flowing gas,[16] and then cooled to ambient conditions before collecting the XAS data. The XAS data were analyzed with the IFEFFIT software and its complementary Athena GUI.[17,18]

Diffuse reflectance UV−vis spectra were acquired using a Fischer Scientific EVO 300 spectrometer equipped with a Praying Mantis reflectance chamber. Spectra were referenced to the diffuse reflectance spectrum of Teflon.

Raman spectra were recorded at ambient conditions using a confocal Raman microscope (LabRam HR, Horiba Jobin Yvon) equipped with a 532 nm HeNe laser operated at a power of 50 mW.

2.4. Theoretical Calculations. The models chosen to represent Ti monomer and dimer active sites are shown in Scheme 1. To mimic the rigidity of the silica support, all geometry optimizations were performed with relaxation of only the Ti atoms, the O atoms in the first coordination sphere, and the H atom of the titanol group. Geometry optimizations and single-point energy calculations were performed using density functional theory (DFT) at the ωB97X-D[19,20]/LANL2DZ and ωB97X-D/CRENBL levels of theory, respectively. Enthalpies at reaction temperature were determined by taking zero point vibrational and temperature corrections into account using the

Scheme 1. Cluster Model of the Tetrahedral (a) Isolated Titanol and the (b) Ti Dimer

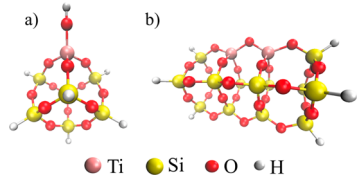

dx.doi.org/10.1021/cs500704b | ACS Catal. 2014, 4, 2908−2916

Table 1. Chemical and Physical Properties of Different *x*-Ti-SBA-15 Catalysts

sample	Si/Ti actual[a]	Ti content (wt %)[a]	Ti dispersion (Ti nm^{-2})	BET surface area (m^2 g^{-1})	pore volume (cm^3 g^{-1})
0.02-Ti−SBA-15	727	0.11	0.016	836	0.75
0.07-Ti−SBA-15	75.5	0.44	0.065	826	0.73
0.3-Ti−SBA-15	43	1.85	0.27	789	0.67
0.7-Ti−SBA-15	17	4.50	0.67	715	0.49
0.07-Ti-Cp/SBA-15		0.42	0.062	805	0.73
0.3-Ti-Cp/SBA-15		1.74	0.26	746	0.63
0.07-Ti-Pr/SBA-15		0.45	0.067	800	0.70
SBA-15				850	0.93

[a]Upon the basis of ICP results.

rigid rotor harmonic oscillator (RRHO) approximation. Entropies were determined using a quasi-RRHO approach proposed by Grimme, which replaces the vibrational entropy for modes with frequencies <100 cm^{-1} by the entropy for a corresponding free-rotor.[21] All calculations were carried out using the Q-Chem software package.[22] The partial charges on atoms were calculated using natural bond orbital (NBO) analysis.[23] The structures of reaction intermediates were hypothesized a priori and then refined by standard geometry optimizations. The transition structures connecting intermediates were found by the freezing-string method[24] followed by local optimization.

3.0. RESULTS AND DISCUSSION

3.1. Catalyst Characterization. The Ti loading, surface area, and pore volume of each catalyst are shown in Table 1. The weight loading was varied from 0.11 to 4.5 wt % in order to change the dispersion of Ti on SBA-15 support. The pore volumes and surface areas of the incorporated and impregnated catalysts for a given Ti weight loading are very similar.

The coordination of Ti in the incorporated Ti−SBA-15 catalysts was probed by X-ray absorption spectroscopy. Previous studies have demonstrated that the pre-edge feature can be used reliably to determine the coordination number of Ti in various oxide compounds.[25] Figure 1 shows the Ti

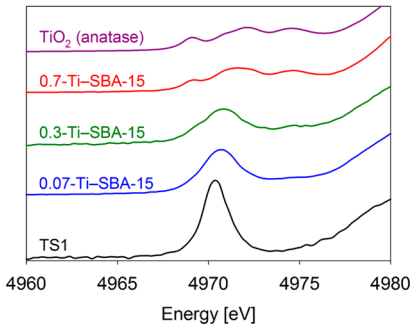

Figure 1. XANES spectra of (−) TS1, (blue line) 0.07-Ti−SBA-15, (green line) 0.3-Ti−SBA-15, (red line) 0.7-Ti−SBA-15, and (purple line) TiO_2 anatase.

XANES region for three samples as well as two Ti standards, TS-1, and TiO_2 anatase. The spectrum of 0.07-Ti−SBA-15 exhibits a single pre-edge feature at 4971 eV similar to that observed in the spectrum of TS-1, indicating that Ti is tetrahedrally coordinated within the framework.[25] The spectrum of 0.3-Ti−SBA-15 has a strong feature at 4971 eV and a small shoulder at 4975 eV, while the spectrum of 0.7-Ti-SBA-15 matches that of bulk TiO_2 anatase. The three peaks at 4969, 4972, and 4975 eV in the spectrum of anatase are due to the transition of 1s core electrons to $1t_{ig}$, $2t_{2g}$, and $3e_g$ molecular orbitals.[26] Thus, the coordination environment of Ti changes from tetrahedral in 0.07-Ti-SBA-15 to distorted octahedral in 0.7-Ti-SBA-15 as the Ti weight loading is increased.

The UV−visible diffuse reflectance spectra of Ti-SBA-15 and TiO_2 anatase are shown in Figure 2. 0.02-Ti-SBA-15 and 0.07-

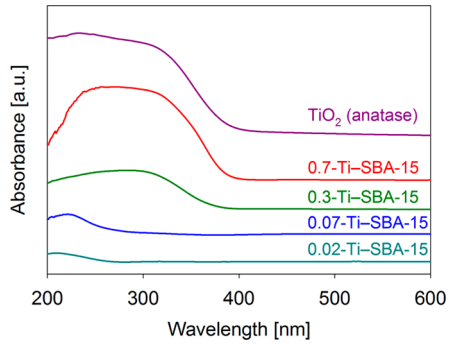

Figure 2. UV−vis spectra of (teal line) 0.02-Ti−SBA-15, (blue line) 0.07-Ti−SBA-15, (green line) 0.3-Ti−SBA-15, (red line) 0.7-Ti−SBA-15, and (purple line) TiO_2 anatase.

Ti-SBA-15 exhibit peaks in the range of 210−230 nm due to the ligand-to-metal charge transfer (LMCT) from oxygen to tetrahedral Ti (IV).[27] Zhao and co-workers have reported that this band provides evidence that Ti is tetrahedrally coordinated and has been incorporated into the framework of SBA-15.[28] As the Ti loading increases, the peak maximum of the absorption is red-shifted to higher wavelengths, approaching that of anatase. Previous studies have reported that this shift can be attributed to partially polymerized hexacoordinated Ti species.[29,30] Consistent with previous UV−visible studies of dispersed TiO_2 nanoparticles on SiO_2, the peak position of the sample containing the highest weight loading of Ti, 0.7-Ti−SBA-15, is blue-shifted from that of anatase due to quantum-size effects.[31,32]

Figure 3 shows the Raman spectra of SBA-15, *x*-Ti-SBA-15, and TiO_2 anatase. The spectrum of SBA-15 exhibits peaks at 485 and 975 cm^{-1}, which are attributed to the stretching vibrations of four-membered siloxane linkages (Si−O−Si) and surface silanol groups (O_3Si−OH), respectively.[33] The spectrum of 0.02-Ti-SBA-15 is indistinguishable from the spectrum of SBA-15 because of the very low weight loading of Ti. The spectrum of 0.07-Ti-SBA-15 exhibits small deviations from the spectrum of pristine SBA-15. The peaks at 485 and 975 cm^{-1} are slightly more intense and broader for 0.07-Ti−SBA-15 than for SBA-15, and a weak peak near 140 cm^{-1} becomes apparent. Similar observations have been reported by

dx.doi.org/10.1021/cs500704b | ACS Catal. 2014, 4, 2908−2916

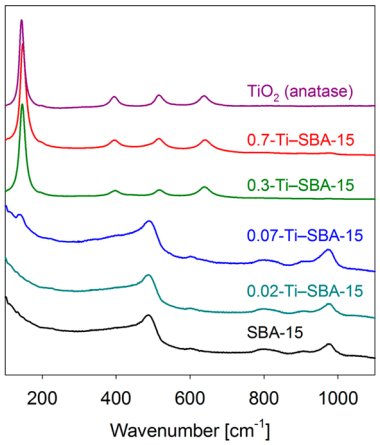

Figure 3. Raman spectra of (black line) SBA-15, (teal line) 0.02-Ti-SBA-15, (blue line) 0.07-Ti-SBA-15, (green line) 0.3-Ti-SBA-15, (red line) 0.7-Ti-SBA-15, and (purple line) TiO_2 anatase.

Turek and co-workers, who observed an increase in the intensity of a peak at 970 cm^{-1} as more Ti was substituted into silicalite.[34] The weak peak around 140 cm^{-1} is the most sensitive fingerprint for anatase and indicates the formation of Ti−O−Ti bonds. Samples with higher Ti loadings than 0.07-Ti-SBA-15 exhibit the four characteristic peaks of anatase at 145, 400, 520, and 650 cm^{-1} due to the E_g symmetric stretching, the B_{1g} symmetric bending, the A_{1g} antisymmetric bending, and the E_g vibrations of Ti−O−Ti bonds, respectively.[35] Although the XRD spectra for these catalysts only indicate the presence of anatase at the highest weight loading (see Supporting Information), the Raman spectra suggest that a fraction of the titanium on the 0.3- and 0.7-Ti-SBA-15 catalysts is present as anatase. This conclusion is based on the recognition that the Raman scattering cross-section of anatase is ∼5-fold greater than that of the isolated TiOx species, which means that the intensities of the Raman peaks for anatase appearing in the spectra are ∼5-fold more intense than what would be expected on the basis of the actual ratio of anatase to isolated TiOx species.

3.2. Catalytic Activity of *x*-Ti−SBA-15 and *x*-Ti/SBA-15 Catalysts. Experiments were conducted under mild conditions to ensure differential conversion so that catalyst deactivation and secondary aldol reactions could be minimized. The only product observed under any of the conditions investigated was the dehydrated aldol product, 2-ethylhexenal. Figure 4 shows

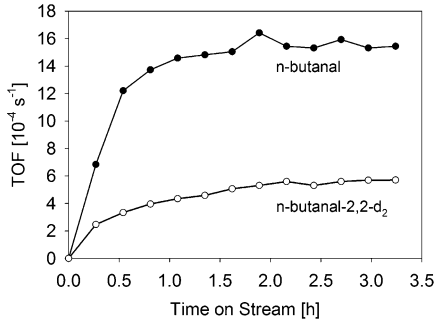

Figure 4. Time on stream study over the 0.02-Ti-SBA-15 catalyst. T = 353 K, P_{Total} = 101.3 kPa, $P_{n\text{-butanal}}$ = 0.2 kPa, (●) *n*-butanal, (○) *n*-butanal-2,2-d_2, and the balance He. Catalyst mass = 0.02 g. Total gas flow rate at STP = 150 cm^3 min^{-1}.

the activity versus time-on-stream for the most active catalyst, 0.02-Ti-SBA-15. After a brief induction period, the catalyst remains stable for at least 3 h. If deuterated, *n*-butanal-2,2-d_2 is reacted over this catalyst, and a kinetic isotope effect of k_H/k_D = 2.5 is observed suggesting that the α C−H bond is involved in the transition state of the rate-limiting elementary step. α-H abstraction is relevant to aldol condensation and will be discussed in the context of the reaction mechanism (see section 3.3).

The activities of *x*-Ti-SBA-15 catalysts are shown in Figure 5. As the weight loading of Ti increases, the turnover frequency

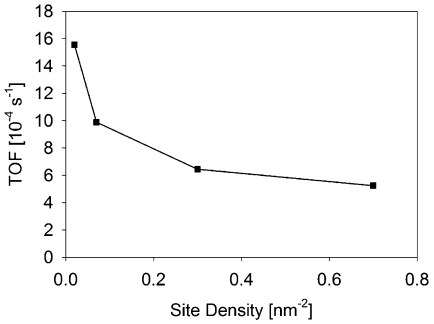

Figure 5. Effect of the Ti site density on the activity of *x*-Ti−SBA-15 catalysts for aldol condensation. T = 353 K, P_{Total} = 101.3 kPa, $P_{n\text{-butanal}}$ = 0.2 kPa, and τ = 4.2 ms (mol Ti/mol feed rate).

decreases monotonically. However, no activity was observed in the absence of Ti. Comparison of the activity of 0.02-Ti-SBA-15 and 0.7-Ti-SBA-15 coupled with the results of the characterization of these samples suggests that isolated tetrahedral Ti sites are more active than hexacoordinated Ti sites. As shown in the Supporting Information, *n*-butanal desorbs at a lower temperature over 0.7-Ti-SBA-15 than 0.07-Ti-SBA-15. Therefore, hexacoordinated Ti sites may be less active than isolated four-coordinated Ti sites because the adsorption of butanal is less favorable at coordinatively saturated sites. A theoretical study comparing the adsorption of formaldehyde onto different Ti sites on the (001) plane of TiO_2 anatase supports this assertion.[36] The results of this study found that the most favorable binding involved the Lewis acid−base interaction between the coordinatively unsaturated Ti (+4) sites and oxygen of the carbonyl group. Hence, the remainder of this study will focus on the more active catalysts containing tetrahedrally coordinated Ti.

Interestingly, the activity of 0.02-Ti-SBA-15 is higher than that of 0.07-Ti-SBA-15 despite the evidence from XANES and UV−visible spectroscopy suggesting that both of these catalysts contain predominantly isolated tetrahedrally coordinated Ti. This finding leads to the proposal that, in addition to the coordination environment, the connectivity of the Ti site also has an effect on the catalytic activity, tetrahedral Ti−O−Ti sites being less active than isolated tetrahedral Ti sites. In order to test this hypothesis, catalysts were synthesized by incipient wetness impregnation using either $Ti(O^iPr)_4$ or Cp_2TiCl_2 precursors. The literature suggests that the latter precursor can be used to synthesize site-isolated catalysts with high Ti loading.[37] However, as shown by entries 2 and 3 of Table 2, the activity of 0.07-Ti-Cp/SBA-15 is two times higher than that of the 0.3-Ti-Cp/SBA-15 catalyst. The TOF values are similar to what was observed in incorporated 0.07-Ti-SBA-15 and 0.3-Ti-SBA-15. Previous experimental and theoretical studies have

dx.doi.org/10.1021/cs500704b | ACS Catal. 2014, 4, 2908−2916

Table 2. Activity (TOF), Apparent Activation Energy (kJ mol^{-1}), and Partial Pressure Dependencies of Ti Silica Catalysts[a]

entry	sample	TOF[b] (10^{-4} s^{-1})	rate[b] (10^{-8} mol g_{cat}^{-1} s^{-1})	activation energy[c] (kJ mol^{-1})	partial pressure dependence[d] (α)
1	0.07-Ti−SBA-15	10.5	2.4	60	0.05
2	0.07-Ti-Cp/SBA-15	11.4	10	59	0.10
3	0.3-Ti-Cp/SBA-15	5.70	21.7	55	0.15
4	0.07-Ti-Pr/SBA-15	2.90	2.7	120	0.20
5	0.07-Ti-Pr/SiO_2-373K	4.05	3.5	61	0.15
6	0.07-Ti-Pr/SiO_2-1023K	8.10	7.3	58	0.10

[a] P_{Total} = 101.325 kPa. [b] T = 353 K, $P_{n\text{-butanal}}$ = 0.2 kPa, and balance He. [c] T = 343−363 K, $P_{n\text{-butanal}}$ = 0.2 kPa, and balance He. [d] T = 353 K, $P_{n\text{-butanal}}$ = 0.1−0.4 kPa, and balance He.

Scheme 2. Mechanism of Aldol Condensation over an Isolated Titanol (R = CH_2CH_3)

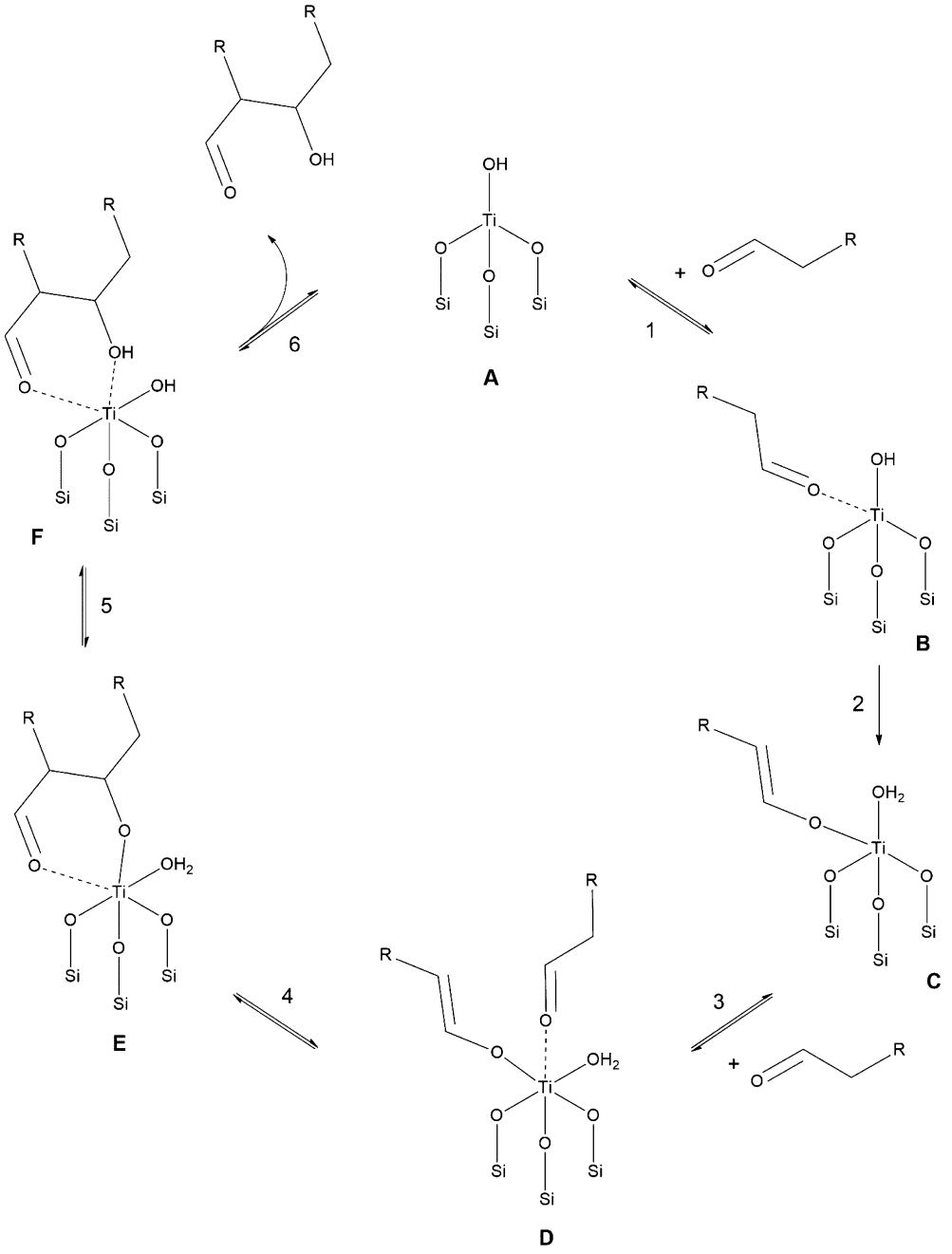

reported that Cp_2TiCl_2 reacts with the silanol groups of mesoporous silica to yield a $(\equiv SiO)_3TiCp$ intermediate, which subsequently forms isolated $(\equiv SiO)_3TiOH$ species after calcination.[16,38] Since the Cp_2TiCl_2 precursor is known to react facilely with the support,[16] and the UV−vis spectra of these catalysts indicates that Ti is tetrahedrally coordinated (see Supporting Information), it is unlikely that the coordination number of Ti changes with loading. However, as the surface

dx.doi.org/10.1021/cs500704b | ACS Catal. 2014, 4, 2908−2916

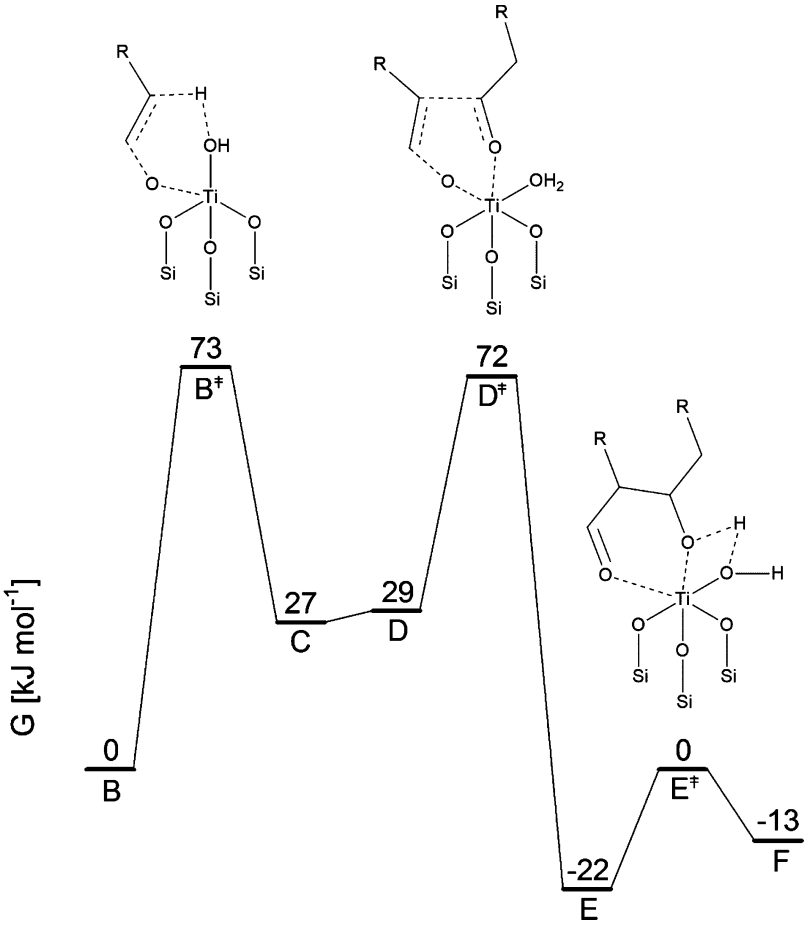

Figure 6. Free-energy (353 K) diagram for aldol condensation over an isolated titanol (where R = H). The elementary steps are labeled according to the reaction mechanism shown in Scheme 2.

density of Ti increases, it is feasible that during calcination neighboring titanols condense to form tetrahedral dimers. Upon the basis of our experimental evidence and previous theoretical studies,[38] the dinuclear Ti species shown in Scheme 1 was chosen to represent the Ti dimer, although other dimer structures may be possible. In accordance with the stated hypothesis, the decrease in activity for catalysts with higher Ti weight loading is attributed to the formation of tetrahedrally coordinated Ti dimers.

Impregnation was also conducted with a $Ti(O^iPr)_4$ precursor because previous literature indicates that this precursor reacts with surface silanol groups to form dinuclear Ti complexes.[39] The probability of forming Ti dimers with this precursor is high since $Ti(O^iPr)_4$ is known to exist as an oligomer in solution.[40] Furthermore, Scott and co-workers have proposed that $Ti(O^iPr)_4$ does not follow simple ligand exchange with the support as other metal precursors do, but rather a grafted Ti monomeric species reacts with $Ti(O^iPr)_4$ to form a dinuclear Ti complex.[39] The UV−vis spectrum of the catalyst synthesized by impregnation of $Ti(O^iPr)_4$ onto SBA-15 shows that Ti is tetrahedrally coordinated (see Supporting Information); however, this catalyst was the least active, as shown by entry 4 of Table 2, supporting the hypothesis that dimers containing tetrahedrally coordinated Ti are less active than tetrahedrally coordinated Ti in monomeric species. Furthermore, the apparent activation energy (as determined from an Arrhenius plot in the temperature interval 343−363 K) for 0.07-Ti-Pr/SBA-15 was 120 kJ mol^{-1}, which is twice that measured for the incorporated 0.07-Ti-SBA-15. Despite the large difference in the apparent activation energy, both catalysts show a kinetic isotope effect (k_H/k_D = 2 is observed over 0.07-Ti-Pr/SBA-15 catalyst), and both are roughly zero order in *n*-butanal.

In an effort to produce isolated Ti species, $Ti(O^iPr)_4$ was impregnated onto amorphous silica pretreated at different temperatures. The purpose of the pretreatment was to dehydroxlate the support in order to spatially separate the silanol groups, thereby increasing the average distance between possible locations at which $Ti(O^iPr)_4$ could graft. The silanol group density was quantified using ^{29}Si MAS NMR as reported previously.[41] Silica pretreated at 373 and 1023 K contains 4 and 1.6 OH nm^{-2}, respectively. As shown by entries 5 and 6 of Table 2, the TOF of 0.07-Ti-Pr/SiO_2-1023K was roughly twice as high as 0.07-Ti-Pr/SiO_2-373K, demonstrating that dehydroxylation of the silica support has a significant effect on the catalytic activity. Similarly, the activity of 0.07-Ti-Pr/SiO_2-373K was greater than that of 0.07-Ti-Pr/SBA-15, indicating that there is an inverse correlation between the activity and the density of silanol groups of the support (SBA-15 contains 5 OH nm^{-2}). Although the Raman spectra of these catalysts exhibit peaks characteristic of anatase, 0.07-Ti-Pr/SiO_2-1023K shows an additional peak characteristic of isolated Ti around 940 cm^{-1} (see Supporting Information). Therefore, the fraction of isolated Ti is dependent upon silanol density. Additionally, the apparent activation energy for 0.07-Ti-Pr/SiO_2 matches that of both the 0.02-Ti-SBA-15 and 0.07-Ti-SBA-15 but is much lower than that of the 0.07-Ti-Pr/SBA-15 catalyst. These

dx.doi.org/10.1021/cs500704b | ACS Catal. 2014, 4, 2908−2916

results suggest that a majority of the catalytic activity for Ti-Pr/SiO_2 occurs at isolated Ti sites, which are more active than tetrahedrally coordinated Ti−O−Ti sites.

3.3. Catalytic Mechanism for Aldol Condensation. The mechanism proposed for aldol condensation over isolated Ti sites is shown in Scheme 2. The reaction sequence begins with the adsorption of butanal via reaction 1. As described previously, the adsorption occurs through a Lewis acid−base interaction between the nucleophilic oxygen of the carbonyl group and the electrophilic Ti (species B). The strength of this interaction polarizes the carbonyl causing the carbon to become more electrophilic and α-H to be more acidic. The increase in acidity facilitates α-H abstraction by the Brønsted base oxygen to form a bound water and enolate intermediate as shown in reaction 2. In reaction 3, the Ti becomes a saturated hexacoordinated species by adsorbing a second molecule of butanal. The polarization of the carbonyl bond induces nucleophilic attack by the enolate to the electrophilic carbon resulting in the formation of a C−C bond in reaction 4. The aldol product is formed in reaction 5 when the bound water acts as a Brønsted acid and desorbs from the active site in reaction 6. Under reaction conditions, the aldol product readily undergoes dehydration to form the thermodynamically favored product 2-ethylhexenal.[11,42]

The kinetic isotope effect observed for both 0.07-Ti-SBA-15 and 0.07-Ti-Pr/SBA-15 provides evidence that enolate formation is a kinetically relevant step. If it is assumed that the adsorption step is quasi-equilibrated, the rate of 2-ethylhexenal formation is given by

$$r_{\text{2-ethylhexenal}} = \frac{K_1 k_2 P_{\text{n-butanal}} L}{1 + K_1 P_{\text{n-butanal}}} \quad (1)$$

where K_1 is the equilibrium constant for reaction 1, k_2 is the rate constant for reaction 2, and L is the number of active sites. The zero-order partial pressure dependence on n-butanal suggests that the surface is saturated with adsorbed aldehyde, and therefore, the rate expression can be simplified to

$$r_{\text{2-ethylhexenal}} = k_2 L \quad (2)$$

suggesting that the apparent activation barrier represents the intrinsic barrier for enolate formation.

3.4. Theoretical Modeling of Tetrahedral Ti Monomer and Ti Dimer Sites for Aldol Condensation. To understand why isolated Ti sites are more active and have a much lower activation barrier than Ti dimer sites, a theoretical analysis of the aldol condensation reaction pathway was performed for both isolated titanol and a dinuclear Ti species. Since the β- and γ-C of n-butanal are inert in aldol condensation and the gas phase deprotonation energy of butanal and ethanal is similar,[43,44] ethanal was used as a model reactant to reduce the computational cost.

Using the isolated titanol cluster, the mechanism shown in Scheme 2 was found to describe the minimum-energy pathway. The changes in Gibbs free energy calculated for the reaction temperature of 353 K are shown in Figure 6, and the changes in enthalpy along the reaction pathway are shown in Figure 7. Since the surface is saturated with adsorbed butanal, as indicated by the zero order partial pressure dependence on n-butanal, the reference state was chosen to include one aldehyde adsorbed to the Ti and another molecule of hydrogen bonded to the hydroxyl of an adjacent silanol. Figure 6 shows that α-H abstraction has the largest free energy barrier in the reaction

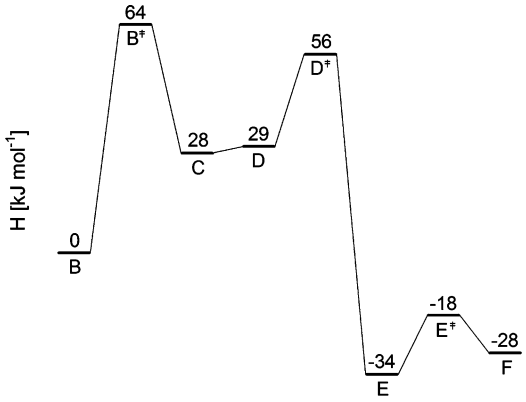

Figure 7. Enthalpy (353 K) diagram for aldol condensation over an isolated titanol (where R = H). The elementary steps are labeled according to the reaction mechanism shown in Scheme 2.

sequence, indicating that enolate formation is the rate-determining step. This conclusion is consistent with the observed kinetic isotope effect. The calculated activation energy for α-H abstraction is 64 kJ mol^{-1}, in good agreement with the value of 60 kJ mol^{-1} determined experimentally. Excellent agreement between theory (123 kJ mol^{-1}) and experiment (120 kJ mol^{-1}) was also found for the barrier of enolate formation over the dinuclear Ti species. Interestingly, the large difference of 60 kJ mol^{-1} in the activation energy between monomer and dimer species cannot be rationalized on the basis of the Lewis acidity of the Ti or the Lewis basicity of the oxygen responsible for the α-H abstraction. As shown in Table 3, the charges on Ti in monomer and dimer species upon

Table 3. Lewis Acid and Base Properties of the Isolated Titanol Monomer and the Ti Dimer

species	charge of Ti (au)	proton affinity (kJ mol^{-1})	$\Delta H^{\ddagger}$ (kJ mol^{-1})
monomer	1.85	−835[a]	64
dimer	1.86	−869[b]	120

[a]Proton affinity of the oxygen of the titanol group. [b]Proton affinity of the oxygen bridge in a Ti−O−Ti dimer.

aldehyde absorption are comparable, indicating that the Lewis acidity of both sites is similar. Even though the calculated proton affinity of the oxygen of Ti−O−Ti is 35 kJ mol^{-1} more basic than the oxygen of titanol, the Ti dimer exhibits a much higher barrier for α-H abstraction. To provide an explanation for this phenomenon, an energy decomposition analysis of the enolate-formation step was performed for the monomer and dimer species. The results of this analysis, shown in Table 4, suggest that the geometric distortion penalty for transitioning from state B to state $B^{\ddagger}$ is 48 kJ mol^{-1} greater for the dimer than for the monomer. Therefore, the activation energy for the dimer is much larger than that for the monomer mainly because

Table 4. Energy Decomposition Analysis of Enolate Formation over Isolated Titanol Monomer and Dimer Species

	geometric distortion energy (kJ mol^{-1})	
species	active site	substrate
monomer	76	144
dimer	52	216

dx.doi.org/10.1021/cs500704b | ACS Catal. 2014, 4, 2908−2916

of geometric constraints. Even though the oxygen of the dimer is a stronger base than that of the titanol, it is less able to readily reach the α-H because of the rigidity of the Ti−O−Ti bridge. Conversely, the titanol is more flexible, resulting in the more facile formation of the enolate.

4.0. CONCLUSIONS

The effects of Ti coordination environment and connectivity on the rate of *n*-butanal self-condensation were investigated over Ti−Si catalysts prepared either by incorporating Ti into the synthesis of SBA-15 to produce Ti-SBA-15 or by grafting Ti onto the surface of preformed SBA-15. Comparison of the rates of aldol condensation for *n*-butanal and *n*-butanal-2,2-d_2 shows an H/D isotope effect of 2.5, indicating that α-H abstraction from an adsorbed butanal is the rate-determining step. The turnover frequency for butanal condensation decreases monotonically with increasing Ti loading, as an increasing fraction of the Ti partitions into oligomers. This change is accompanied by an increase in the apparent activation energy from 55 to 60 kJ mol^{-1} for monomeric Ti species to 120 kJ mol^{-1} for oligomeric species.

Theoretical analysis of the aldol mechanism over an isolated titanol group demonstrates that α-H abstraction from an adsorbed alkanal is the rate-determining step, consistent with the observed kinetic isotope effect. The calculated activation barrier for enolate formation over isolated titanol, 64 kJ mol^{-1}, is in very good agreement with what is measured experimentally. An estimate of the activation barrier for enolate formation over Ti dimer species led to an activation energy of 123 kJ mol^{-1}, in good agreement with the value measured for a catalyst containing oligomeric species. Energy decomposition analysis of the enolate formation step shows that although the oxygen present on the Ti−O−Ti of the dimer species is more basic than the oxygen of the Ti monomer species, there is a larger energetic penalty for the substrate to distort over the Ti−O−Ti dimer. The oxygen of the titanol is less rigid and is therefore able to bend more easily to abstract the α-H and form the enolate.

■ ASSOCIATED CONTENT

Supporting Information

XRD of *x*-Ti−SBA-15; TGA scans of *n*-butanal; UV−vis spectra of 0.07-Ti-Cp/SBA-15, 0.3-Ti-Cp/SBA-15, and 0.07-Ti-Pr/SBA-15; Raman spectra of 0.07-Ti-Pr/SiO_2-373K and 0.07-Ti-Pr/SiO_2-1023K; and TEM image of 0.3-Ti−SBA-15. This material is available free of charge via the Internet at http://pubs.acs.org.

■ AUTHOR INFORMATION

Corresponding Author

*Tel: +1 510 642 1536. Fax: +1 510 642 4778. E-mail: bell@cchem.berkeley.edu.

Notes

The authors declare no competing financial interest.

■ ACKNOWLEDGMENTS

This work was supported by the XC^2 program funded by BP. We thank the Professor T. Don Tilley for providing TS-1 and Eric Bloch for his assistance in performing TGA.

■ REFERENCES

(1) Lee, G-S. J.; McCain, J. H.; Bhasin, M. M. Synthetic Organic Chemicals. In *Handbook of Industrial Chemistry and Biotechnology*, 11th ed.; Kent, J. A., Ed.; Springer, New York, 2010; Vol. *1*, pp 345−403.
(2) Arena, B. J.; Holmgren, J. S. Direct Conversion of Butyraldehyde to 2-Ethylhexanol-1. US5258558 A, Nov. 2, 1992.
(3) Kiss, A. A.; Dimian, A. C.; Rothenberg, G. *Adv. Synth. Catal.* **2006**, *348*, 75−81.
(4) Knothe, G.; Matheaus, A. C.; Ryan, T. W., III *Fuel* **2003**, *82*, 971−975.
(5) Tanabe, K. *J. Chin. Chem. Soc.* **1998**, *45*, 597−602.
(6) Tanabe, K.; Yamaguchi, T. *Catal. Today* **1994**, *20*, 185−198.
(7) Shylesh, S.; Thiel, W. R. *ChemCatChem* **2011**, *3*, 278−287.
(8) Iglesia, E.; Barton, D. G.; Biscardi, J. A.; Gines, M. J. L.; Soled, S. L. *Catal. Today* **1997**, *38*, 339−360.
(9) Noziere, B.; Cordova, A. *J. Phys. Chem. A* **2008**, *112*, 2827−2837.
(10) Rekoske, J. E.; Barteau, M. A. *Ind. Eng. Chem. Res.* **2011**, *50*, 41−51.
(11) Singh, M.; Zhou, N.; Paul, D. K.; Klabunde, K. J. *J. Catal.* **2008**, *260*, 371−379.
(12) Idriss, H.; Barteau, M. A. *Catal. Lett.* **1996**, *40*, 147−153.
(13) Idriss, H.; Kim, K. S.; Barteau, M. A. *J. Catal.* **1993**, *139*, 119−133.
(14) Kruk, M.; Cao, L. *Langmuir* **2007**, *23*, 7247−7254.
(15) Kelly, S. D.; Hesterberg, D. Analysis of Soils and Minerals Using X-ray Absorption Spectroscopy. In *Methods of Soil Analysis: Mineralogical Methods, Part 5*; Ulery, A. L., Drees, L. R., Eds.; American Society of Agronomy: Madison, WI, 2008; pp 378−464.
(16) Jentoft, R. E.; Deutsch, S. E.; Gates, B. C. *Rev. Sci. Instrum.* **1996**, *67*, 2111−2112.
(17) Ravel, B.; Newville, M. *J. Synchrotron Radiat.* **2005**, *12*, 537−541.
(18) Newville, M. *J. Synchrotron Radiat.* **2001**, *8*, 96−100.
(19) Chai, J.-D.; Head-Gordon, M. *Phys. Chem. Chem. Phys.* **2008**, *10*, 6615−6620.
(20) Chai, J.-D.; Head-Gordon, M. *J. Chem. Phys.* **2008**, *128*, 084106−084115.
(21) Grimme, S. *Chem.—Eur. J.* **2012**, *18*, 9955−9964.
(22) Shao, Y.; Molnar, L. F.; Jung, Y.; Kussmann, J.; Ochsenfeld, C.; Brown, S. T.; Gilbert, A. T. B.; Slipchenko, L. V.; Levchenko, S. V.; O'Neill, D. P.; DiStasio, R. A., Jr.; Lochan, R. C.; Wang, T.; Beran, G. J. O.; Besley, N. A.; Herbert, J. M.; Lin, C. Y.; Van Voorhis, T.; Chien, S. H.; Sodt, A.; Steele, T. P.; Rassolov, V. A.; Maslen, P. E.; Korambath, P. P.; Adamson, R. D.; Austin, B.; Baker, J.; Byrd, E. F. C.; Dachsel, H.; Doerksen, R. J.; Dreuw, A.; Dunietz, B. D.; Dutoi, A. D.; Furlani, T. R.; Gwaltney, S. R.; Heyden, A.; Hirata, S.; Hsu, C.-P.; Kedziora, G.; Khalliulin, R. Z.; Klunzinger, P.; Lee, A. M.; Lee, M. S.; Liang, W. Z.; Lotan, I.; Nair, N.; Peters, B.; Proynov, E. I.; Pieniazek, P. A.; Rhee, Y. M.; Ritchie, J.; Rosta, E.; Sherrill, C. D.; Simmonett, A. C.; Subotnik, J. E.; Woodcock, H. L., III; Zhang, W.; Bell, A. T.; Chakraborty, A. K.; Chipman, D. M.; Keil, F. J.; Warshel, A.; Hehre, W. J.; Schaefer, H. F., III; Kong, J.; Krylov, A. I.; Gill, P. M. W.; Head-Gordon, M. *Phys. Chem. Chem. Phys.* **2006**, *8*, 3172−3191.
(23) Foster, J. P.; Weinhold, F. *J. Am. Chem. Soc.* **1980**, *102*, 7211−7218.
(24) Behn, A.; Zimmerman, P. M.; Bell, A. T.; Head-Gordon, M. *J. Chem. Phys.* **2011**, *135*, 224108.
(25) Farges, F.; Brown, G. E., Jr.; Rehr, J. J. *Phys. Rev. B* **1997**, *56*, 1809−1819.
(26) Hwang, J.-S.; Chang, J.-S.; Park, S.-E.; Ikeue, K.; Anpo, M. *Top. Catal.* **2005**, *35*, 311−319.
(27) Jarupatrakorn, J.; Tilley, T. D. *J. Am. Chem. Soc.* **2002**, *124*, 8380−8388.
(28) Li, G.; Zhao, X. S. *Ind. Eng. Chem. Res.* **2006**, *45*, 3569−3573.
(29) Blasco, T.; Corma, A.; Navarro, M. T.; Perez Pariente, J. *J. Catal.* **1995**, *156*, 65−74.
(30) Petrini, G.; Cesana, A.; De Alberti, G.; Genoni, F.; Leofanti, G.; Padovan, M.; Paparatto, G.; Roffia, P. *Stud. Surf. Sci. Catal.* **1991**, *68*, 761−766.

(31) Fernandez, A.; Leyrer, J.; Gonzalez-Elipe, A. R.; Munuera, G.; Knozinger, H. *J. Catal.* **1988**, *112*, 489−494.
(32) Luan, Z.; Kevan, L. *J. Phys. Chem. B* **1997**, *101*, 2020−2027.
(33) Laun, Z.; Maes, E. M.; van der Heide, P. A. W.; Zhao, D.; Czernuszewicz, R. S.; Kevan, L. *Chem. Matt.* **1999**, *11*, 3680−3686.
(34) Deo, G.; Turek, A. M.; Wachs, I. E.; Huybrechts, D. R. C.; Jacobs, P. A. *Zeolites* **1993**, *13*, 365−373.
(35) Yan, J.; Wu, G.; Guan, N.; Li, L.; Li, Z.; Cao, X. *Phys. Chem. Chem. Phys.* **2013**, *15*, 10987−10988.
(36) Liu, H.; Wang, X.; Pan, C.; Liew, K. M. *J. Phys. Chem. C* **2012**, *116*, 8044−8053.
(37) Calleja, G.; van Grieken, R.; Garcia, R.; Melero, J. A.; Iglesias, J. *J. Mol. Catal. A* **2002**, *182*−*183*, 215−225.
(38) Sinclair, P. E.; Sankar, G.; Catlow, C. R. A. *J. Phys. Chem. B* **1997**, *101*, 4232−4237.
(39) Omar Bouh, A.; Rice, G. L.; Scott, S. L. *J. Am. Chem. Soc.* **1999**, *121*, 7201−7210.
(40) Sharpless, K. B.; Woodard, S. S.; Fin, M. G. *Pure Appl. Chem.* **1983**, *55*, 1823−1836.
(41) Shylesh, S.; Hanna, D. G.; Werner, S.; Bell, A. T. *ACS Catal.* **2012**, *2*, 487−493.
(42) McMurry, J. Dehydration of Aldol Products: Synthesis of Enones. In *Organic Chemistry*, 6th ed.; Thomson Learning: Pacific Grove, CA, 2004; pp 859−860.
(43) Acetaldehyde. http://webbook.nist.gov/cgi/cbook.cgi?ID=C75070&Units=SI&Mask=8#Thermo-React (accessed Mar 17, 2014).
(44) Butanal. http://webbook.nist.gov/cgi/cbook.cgi?ID=C123728&Units=SI&Mask=8#Thermo-React (accessed Mar 17, 2014).